PFC/RR-84-1 DOE/ET/51013-111
UC20

THE VERSATOR DIVERTOR EXPERIMENT: PRELIMINARY DESIGNS*

Alan S. Wan, T. F. Yang

Plasma Fusion Center
Massachusetts Institute of Technology
Cambridge, Massachusetts 02139 USA

August 1984

*This work was supported by the US Department of Energy under Contract # DE-AC02-78ET-51013. Reproduction, translation, publication, use and disposal, in whole or part, by or for the United States government is permitted.

THE VERSATOR DIVERTOR EXPERIMENT: PRELIMINARY DESIGNS

Alan S. Wan, T. F. Yang

Plasma Fusion Center
Massachusetts Institute of Technology
Cambridge, Massachusetts 02139 USA

ABSTRACT

The emergence of magnetic divertors as an impurity control and ash removal mechanism for future tokamak reactors brings on the need for further experimental verification of the divertor merits and their ability to operate at reactor relevant conditions, such as with auxiliary heating. This paper presents preliminary designs of a bundle and a poloidal divertor for Versator II, which can operate in conjunction with the existing 150 kW of LHRF heating or LH current drive. The bundle divertor option also features a new divertor configuration which should improve the engineering and physics results of the DITE experiment. Further design optimization in both physics and engineering designs are currently under way.

I. Introduction

In the process of commercial realization of fusion reactors, the question of impurity control becomes more and more prominant as each new experimental device reaches for higher and higher density, temperature, and confinement time. Extrapolating the high-z impurity concentration of present day experiments to future reactor conditions, the energy loss due to line and bremsstrahlung radiation would exceed the fusion energy released, thus quenching the burn [1]. Besides impurities, another by-product of the D-T reaction is the helium ash. Ash buildup due to insufficient removal mechanism would lead to reduce fusion reaction rate and eventually would also quench the burn. Therefore, it is essential to find an effective scheme for impurity control and ash removal.

For tokamak applications, pump limiters and magnetic divertors are the primary candidates to fill such a role. The pump limiter behaves like a "scoop" which neutralizes incoming charged particles in the scrape-off layer and removes these particles through a pumping duct behind the limiter. The main drawback of using pump limiters is its direct contact with the plasma. Questions concerning the sensitivity of edge plasma parameters on material erosion rate [2] and the rate and mechanism of limiter material redeposition [3] make pump limiters an alternative that needs experimental supports which are currently under way at PDX [4], ISX-B [5], and TEXTOR [6].

The basic problem of direct plasma-surface interactions inside the vacuum chamber is avoided by means of a magnetic divertor. In a divertor configuration, the charged particles diffuse across the separatrix surface defined by the divertor as a magnetic limiter and particles flow along

the diverted field lines into the divertor chamber where they are neutralized on the target and pumped away. If the scrape-off layer is thick and dense enough, neutral impurities will likely be ionized and removed before reaching the plasma. Likewise, most charged particles and energy flux from the main plasma are removed before reaching the wall, thus reducing the wall loading. Therefore, besides controlling impurities and removing ashes, the divertor can also eliminate the need of limiters and ease the first wall material requirements.

Tight aspect ratio toroidal devices such as tokamaks can consider two different divertor configurations: poloidal and bundle divertors. The poloidal divertor coils run concentric with the discharge and generate an axisymmetric separatrix surface by producing a cancelling poloidal field. The bundle divertor is a modification of the toroidal divertor. It produces a highly localized distortion of the toroidal field and leads a bundle of flux into the divertor chamber.

Like the pump limiters, the verdict is still out on the true merits of the divertor. More experimental evidences are necessary. In Section II we will briefly review the up-to-date bundle and poloidal divertor experimental results. The objective of this paper is to present initial designs of a bundle divertor experiment (Section III) and a poloidal divertor experiment (Section IV) on Versator II. As the name Versator implied, it is a very versatile tokamak experiment, requiring little or no machine modifications in adopting the divertor experiments. Coupled with the present lower hybrid heating and current drive experiments, we can also study the effect of the divertors on auxiliary heating, especially on the issues of fast ion confinement, (non)presence of impurity on

heating efficiency, and the sensitivity of edge parameters on rf accessibility. The basic Versator machine and plasma parameters are presented in Table I. Other relevant parameters concerning the divertor designs will be presented in the appropriate sections.

II. Review of Divertor Experiments

Lyman Spitzer first conceived the concept of a divertor on stellarators in 1951 [7,8]. The usefulness of divertors to reduce radiation losses was demonstrated shortly afterward by Bennet, et al. [9] in 1958. However, early divertor configurations were in the form of toroidal divertors which could not be utilized on the tight aspect ratio tokamaks. It was not until recently when the fusion community began to seriously consider the feasibility of long-pulsed reactors that the divertors received further attention.

One of the earliest poloidal divertor experiments was done on FM-1 Spherator [10], which was a toroidal internal ring at PPPL. The first poloidal divertor experiments on tokamaks were done on DIVA [11] and T-12 [12], both operated at a plasma current of about 40 kA. Both experiments experienced high particle exhaust efficiency (~ 100% T-12; ~ 75% DIVA). Concentration of impurities were significantly reduced by 25-50% on DIVA when the divertor was turned on. DIVA also exhibited excellent impurity screening efficiency of 50-70%. Both machines also observed significant reduction in radiated power loss when the divertor was operating (~ 60% reduction in T-12; 25-50% in DIVA).

Larger scale (~ 500 kA I_p) experiments such as PDX [13], ASDEX [14, 15], and Doublet III [16] soon followed. Another experiment, JT-60, is

still currently under construction. The Doublet III device was originally designed to have an elongated type of plasma configuration. In converting to a single null divertor experiment, there is no specific target chamber. It was found on both ASDEX and PDX [9] that the closed poloidal divertor geometry, which leads to high boundary density and pressure, has clearly the potential for high particle exhaust and energy collection efficiencies. Both devices observed the presence of H-mode regimes during neutral beam discharges. Energy confinement time, τ_E, was found to scale linearly with I_p for these devices. τ_E of values up to 55 ms was measured on PDX while ASDEX attained values up to 70 ms for D_2 discharges and 35 ms for H_2 discharges. They have demonstrated the ability to reduce impurity source sufficiently such that clean plasmas can be produced even for megawatt level of auxiliary heating.

The bundle divertor was first proposed by Colven, Gibson and Stott in 1972 [18]. The only bundle divertor experiment on tokamaks is done on DITE [19,20] at Culham Laboratory in England. DITE has installed a series of three bundle divertor experiments (MKIA, MKIB, MKII) starting from 1976. Each successive divertor is designed to handle better plasma parameters and various wall and operating conditions. For example, MKIA operated at 50 kA plasma current and 1.0 Tesla toroidal field on axis, whereas MKII can operate at 250 kA plasma current and up to 2.7 Tesla toroidal field on axis.

The overall results were quite reasonable. MKIA was able to attain high particle exhaust (~ 30%) and energy collection (~ 80%) efficiencies while maintaining good impurity screening and reduction capability that attain the level comparable to that of DIVA. MKIB operated with titanium

limiters and titanium gettering of the walls. It also worked with predominantly deuterium discharges and at higher plasma temperature, density, current and toroidal field than MKIA. The MKIB results were significantly worse than MKIA results in all phases of divertor efficiency diagnostics. The differences may be attributed to different operating conditions or different physics interpretations. Both divertor experiments, however, showed no evidence of divertor caused flux surface ergodicity or enhanced particle loss.

The MKII divertor modified the original MKI designs by decreasing the angle between divertor field coils and changing the divertor cross section. These changes allow the divertor to operate at high plasma conditions and toroidal field intensity. MKII also employed graphite limiters instead of titanium and glow discharge cleaning instead of titanium gettering. The preliminary results showed that about 50% of the nonradiated ohmic power is transferred to the target plate, and better efficiencies are expected at higher edge density, collisional edge regime. MKII also found the underlying transport mechanism is independent from the heating method.

III. The Versator Bundle Divertor Experiment

Despite the initial success of the DITE bundle divertor experiments, several critical physics and engineering issues remain unsolved.

On the engineering side, the key issues concern the conductor current density limit and the actual physical size of the entire bundle divertor assembly. The two issues are mutually dependent. Earlier studies [21,22, 23] have demonstrated the sensitivity of the required divertor current on

the geometric parameters. In general, larger divertors lead to reduced current density which eases the thermal hydraulics and force criterions. However, it is also desirable to have plug-in type bundle divertors in order to offer easier maintenance and replacement. It is difficult to meet both goals simultaneously.

Physically, the DITE MKI and MKII divertors are not plug-in devices. They fit in between the TF coils and the vacuum chamber. This design enables the DITE divertors to operate at an acceptable current density range, which is about 20 kA/cm^2-Tesla. Extrapolating to reactor conditions, this current density requirement will impose severe engineering problems in both thermal hydraulics and power requirements. Another problem that results from the high current density is the high $\underline{j} \times \underline{B}_T$ forces on the divertor coils. Larger force requires more structural support which once again brings us back to a physically larger divertor.

The main concern among the physics issues is the effect of divertor field perturbation on fast ion confinement. The DITE divertors have already demonstrated the effectiveness of bundle divertors in satisfying the functions of plasma exhaust and screening, first wall unloading, and plasma boundary control [19,20]. However, they also created large field perturbation inside the plasma. The ripple on-axis during divertor operation reaches as high as 3-4%, where ripple (ε) is defined as

$$\varepsilon(r,\theta,z) \equiv |B_{max} - B_{min}|/|B_{max} + B_{min}| \ , \qquad (1)$$

where B_{max} and B_{min} are, respectively, the maximum and minimum field intensity along the field line launched at (r,θ,z). Here the ripple profile is calculated by launching field lines from the $\phi = 0°$ axis, where the

$\phi = 0°$ half plane divides the bundle divertor into two symmetric halves toroidally.

The presence of large divertor ripple creates perturbation to the magnetic surfaces, thus producing ergodic surfaces which destroy charged particle confinement. Transport wise, the presence of divertor ripple well yields a new ripple-trapping mechanism [24]. Therefore banana-trapped particles can become trapped in this well and quickly drift out of the tokamak [23,25]. Furthermore, the stagnation axis of the DITE bundle divertors [24,26] concaves away from the plasma surface contour. This behavior caused larger off-axix ripple and larger perturbed plasma volume.

Another important divertor physics parameter is the divertor acceptance angle, χ_D, and the frequency of diversion, q_D, defined by

$$q_D \equiv 2\pi/\chi_D \ . \qquad (2)$$

q_D is interpreted physically as the mean number of turns of a field line in the scrape-off region around the torus before being diverted into the divertor chamber. Typically, DITE bundle divertors operated at $q_D \sim 6$-7 [26]. Smaller q_D is desired in order to allow thinner scrape-off layer and better overall divertor performances.

III.1 The Versator II Bundle Divertor Design

The Versator II bundle divertor is designed to offer possible solutions to the engineering and physics questions left by the DITE bundle divertors. It employs the advanced 3-T cascade design [21] with modified arc shaped coils [27,28] instead of the conventional straight T coils. A single T shaped arc coil is illustrated in Figs. 1a-1c. As demonstrated

in these figures, the arc segments are contoured to fit the plamsa both toroidally and poloidally. This change brings two improvements over the straight T coils. First, most part of the coils are now closer to the plasma, reducing the total current requirement to achieve the same separatrix. More importantly, the new stagnation axis now conforms with the plasma shape, lowering the field perturbation inside the plasma, thus offering much better overall fuel ion confinement. By increasing the poloidal sections of the divertor arcs, this new divertor configuration appears more like a toroidal hybrid bundle divertor [27]. In combination with the change of stagnation axis contour, more scrape-off fluxes are diverted into the divertor chamber, thus reducing q_D and subsequently we have a more efficient divertor configuration.

Cascading the three T shaped arc coils together, we now have the basic configuration of the new advanced bundle divertor for Versator II.

Basically five geometric parameters must be adjusted during the configuration optimization procedure. They are illustrated in Fig. 2 and are described below. x_o, the radial distance to the imaginary center of the leading y-z surface; x_ℓ, the length in x direction; y_ℓ, the half width in y direction; z_ℓ, the total height; and x_c, the coil cross section. All distances are measured from the coil center obtained by imagining a filament in place of the actual finite coil. Reference 21 gives a detailed geometric optimization study of these five parameters using the straight T coils and projected reactor conditions. Due to the geometric constraint of the Versator, the maximum z_ℓ and y_ℓ are fixed by the largest side port dimension of 6" × 12". Typically we want x_ℓ and x_o to be small in order to bring the divertor coils closer to the plasma,

thus reducing the total divertor current required to achieve the separatrix. However, x_o must be sufficiently large such that the closest coils produce acceptable field line distortion. x_ℓ must be large enough in order to maintain a large divertor chamber besides the coil and structure. x_c is picked based on the desired operating current density. It also plays a role in the actual positioning of the coils.

The final divertor configuration is chosen based on geometric constraints, thermal hydraulics requirements, force constraints, separatrix location and shape, and the effect of the divertor on plasma perturbation. We used four separate codes in determining the impact of a specific divertor configuration on all these considerations. PEST [29], the Princeton Equilibrium Stability and Transport Code, is used to obtain the Versator 2-D plasma equilibrium profile. TCAN [30], for Time-dependent incompress ible-flow Conductor ANalysis, is used to predict the thermal hydraulics aspect of the design. EFFI [31], a code for calculating the Electrostatic Field, Force and Inductance in coil systems of arbitrary geometry, is used to determine the total force and torque on the entire divertor and expansion coil set. MAFCO [31], for MAgnetic Field COde, is used as a general purpose magnetic field line following code to determine the separatrix shape and location. Coupling MAFCO and PEST, we can determine the ergodicity of flux surface inside the separatrix.

The first step of the divertor design procedure is to find the magnetic configuration that satisfies both the geometric constraints and plasma separatrix location. Low current density and large flux expansion near the target are also desirable qualities. This step is carried out using MAFCO.

The magnetic configuration of the intital bundle divertor obtained for Versator II is shown in Fig. 3. Table II lists the divertor parameters in terms of the geometric variable mentioned above and the required current per coil. The separatrix yields a maximum plasma boundary of 53.5 cm. The rest of the operating conditions are listed in Table I. The poloidal cross section of the plasma, the machine, and the divertor are shown in Fig. 4 Notice that a large expansion coil is added at the end of the 3-T divertor assembly. This expansion coil expands the separatrix to beyond the TF coil radius. With the help from the TF coils as additional expansion coils, the final separatrix appears well expanded in order to reduce the thermal loading on the target and increase the pumping efficiency.

As shown in Fig. 4, the Versator side port extends out to a major radius of 60 cm. Therefore, for the three divertor coils there is a maximum size limit of 6" (width) × 12" (height). The expansion coil can be larger but it is still limited by the TF coil separation. During the experiment, the entire divertor assembly, including the expansion coil and target, must be enclosed in a vacuum housing. However, the Versator II bundle divertor can be a plug-in unit, requiring no further machine modification.

The Versator II 2-D plasma equilibrium profile is calculated using PEST. The flux surfaces are plotted out in Fig. 5. We can recover the poloidal and vertical field information from this unperturbed plasma profile. Coupling with the toroidal and divertor field information by MAFCO input, we can follow field lines around the torus for a couple of hundred turns and map out a puncture plot exhibiting the flux surface

characteristics. Figures 6 and 7 show the flux surface structures when the Versator II bundle divertor is turned on. Notice that all surfaces within the separatrix are nonergodic. The field lines started in the scrape-off region are highly ergodic. They are diverted within a few transits around the plasma poloidally.

Another way to examine the effect of divertor perturbation is to calculate the ripple along the $\phi = 0°$ axis. These ripple values are plotted out in Fig. 8 as a function of major radius. Notice that the absolute value of ripple on axis is only 0.7%, quite a bit smaller than the DITE bundle divertors. The ripple values for the Versator bundle divertor are higher than the similar type of arc bundle divertors designed for TEXTOR, DITE, and INTOR. The larger ripple can be attributed to limited machine access which leads to smaller divertors at higher field and causes larger ripple values. A direct comparison of the DITE-type and advanced T-shaped cascade-type divertors in a separate study [33] has also confirmed the superior ripple profile of this new design. With the properly contoured stagnation axis, the overall perturbed plasma volume is decreased dramatically. Therefore, the new Versator divertor configuration offers a much improved design in both divertor efficiency and confinement physics.

The thermal hydraulics analysis of the Versator bundle divertor is carried out using TCAN, a time dependent incompressible flow code that enables us to determine the overall energy requirement, the instantaneous power, the coil temperatures, and the overall pressure drop. For convenience sake, the inlet coolant conditions approximates that of the off-the tap water. Specific coolant and conductor conditions are listed in Table III.

In the Versator analysis we break up the conductors into four turns per coil. Figure 9 shows the cut-away cross section of the divertor coil. All turns are insulated from each other with 1 mm insulators. The coolant runs through a cylindrical coolant duct occupying about 10% of the total conductor cross sectional area. In matching with the Versator operating conditions, the divertor is turned on for 100 ms flat-top, with 20 ms each to ramp the current up to maximum and decay down from the maximum back to zero.

The results of the thermal hydraulics analysis is tabulated in Table IV. The time history of the temperature at the coolant entrance, middle of coil, and coolant sxit of the middle divertor coil is shown in Fig. 10. Notice that neither the temperature rise in the conductor nor the pressure drop per turn appears unreasonable. The most important result in this analysis is to determine the total energy required to run the divertor. We expect to use the present capacitor bank at Versator as our power supply. Therefore, total energy required becomes a more important parameter than the instantaneous power requirement. This preliminary divertor design requires a total of 150 kJ. The expansion coil requires significantly more energy than any single divertor coil. This is because of its large total conductor volume and high current density, which is the same as the divertor coil current density after excluding the insulation and coolant area.

The final step of the design procedure utilizes the EFFI code to calculate the $\underline{J} \times \underline{B}$ forces imposed on the divertor assembly. Two dominant sources of magnetic field are present in this design: the toroidal field and the self-imposing divertor field. The forces on the divertor coil

assembly can be broken down to two major forces as shown in Fig. 11. An outward radial force of 11.3 kN is applied on the entire assembly. Furthermore, bending torques of strength 102 kN-m and 52 kN-m are imposed on the main divertor coils (as a unit) and the expansion coils respectively. Both the radial force and the bending torques can be easily handled without major structural requirements.

IV. The Versator Poloidal Divertor Experiment

One important aspect of the divertor physics that has not been investigated in the previous poloidal divertor experiments is the coupling of divertor operation with auxiliary rf heating. ASDEX Upgrade [34] is proposing a large scale poloidal divertor experiment with 12 MW ICRF heating and current drive so they can study the effect of reactor-like power flux density in the plasma boundary of ~ 0.3 MW/m^2. With slight modification, we propose to add a poloidal divertor onto Versator II in order to study the effect of a poloidal divertor on LHRF heating.

The poloidal divertor design is carried out by using PEST [29]. We input the present Versator coil scheme and added a poloidal coil that fits inside the square-shape vacuum chamber (see Fig. 4). The Versator parameters are listed in Table I. In searching for a satisfactory double null divertor configuration, we can adjust the following parameters: divertor current, divertor positions, and profile factors β_p and β_g, for the pressure function $p(\psi)$ and g-function $g(\psi)$ respectively. $g(\psi)$ is proportional to the poloidal current passing through the surface bounded by r = constant and z = 0, where (r,θ,z) formed the toroidal coordinates. ψ is the poloidal flux, p and g functions are free functions defined [29,35] as

$$p(\psi) = P_o \left(\frac{\psi - \psi_o}{\psi_L - \psi_o} \right)^{\beta_p} \text{ and} \tag{3}$$

$$g(\psi) = 1 - g_p \left(\frac{\psi - \psi_o}{\psi_L - \psi_o} \right)^{\beta_g} \tag{4}$$

P_o is the peak pressure and g_p is proportional to the plasma dielectric constant. ψ_o and ψ_L are the poloidal magnetic flux at the magnetic axis and limiter, respectively.

The preliminary poloidal divertor coil parameters and the parameters of the equilibrium coils are listed in Table V. Figure 12 shows a poloidal cross section of the flux surfaces when the divertor is turned on. Further optimization is necessary and the engineering analysis is yet to be done. These works are presently under way.

V. Conclusion

Thus far the preliminary experimental results have shown the magnetic divertors to be a promising scheme to control impurities and limit plasma boundary. However, major engineering and physics questions remain unanswered. One important unfulfilled goal is the effect of the divertor on rf auxiliary heating. In this paper we proposed preliminary designs of a bundle divertor and a poloidal divertor experiment on Versàtor II, which presently has capability of launching 150 kW of lower hybrid waves to study both heating and current drive.

Besides being the first bundle divertor experiment to study the coupled operation with lower hybrid heating and current drive, the Versator bundle divertor also represents a superior design than the DITE

experiments in both divertor physics and engineering requirements. The divertor is designed as a plug-in device operating at much lower current density and stress on coils. Thermal hydraulics and force requirements are well within the technology limits. The stagnation axis now concaves toward the plasma contour. The ripple profile on $\phi = 0$ axis is comparatively lower than DITE and the acceptance angle can be increased by over 50%. These results suggested that the divertor now operates with a much smaller perturbed plasma volume. This conclusion was validified by studying the ergodicity of the flux surfaces both inside and outside the separatrix surface.

The poloidal divertor design is still under way. Preliminary results demonstrated the ease of installing a poloidal divertor on Versator without much modification. However, further optimization is still necessary in both the physics and engineering designs.

Needless to say, much work remains before a bundle or poloidal divertor experiment can actually take place on Versator. This report provides a basis to initiate the next phase of design. It is realistic to assume that only one type of divertor will be put on Versator. We should decide on the proper option to do a detail design study. Presently we are preparing a 3-D Monte Carlo guiding center code to study the charged particle behavior and transport mechanisms in the presence of a divertor. Proper diagnostics must be chosen and tested in order to document the effectiveness of the divertor. And finally, a mock-up divertor should be built to test the code accuracy in both magnetics and thermal hydraulics.

REFERENCES

[1] D. M. Meade, Nuclear Fusion, 14 (1974) 289.

[2] P. J. Gierszewski, "Plasma/Neutral Transport in Divertors and Limiters," PFC/RR-83-28, August 1983.

[3] J. Brooks, et al., US FED-INTOR Activity Report, Critical Issues, Vol. 1, 1982, ch. 6,7.

[4] R. Budny, et al., "Initial Results from the Scoop Limiter Experiment in PDX," Symposium on Energy Removal and Particle Control in Toroidal Fusion Devices, July 26-29, 1983, Princeton, NJ; Journal of Nuclear Materials 121 (1984) pp. 294-303.

[5] P. Mioduszewski, et al., "Particle Removal with Pump Limiters in ISX-B," Symposium on Energy Removal and Particle Control in Toroidal Fusion Devices, July 26-29, 1983, Princeton, NJ; Journal of Nuclear Materials 121 (1984) pp. 285-293.

[6] Various papers in Symposium on Energy Removal and Particle Control in Toroidal Fusion Devices, July 26-29, 1983, Princeton, NJ; Journal of Nuclear Materials 121 (1984).

[7] L. Spitzer, "A Proposed Stellarator," AEC Report No. NYO-993 (PM-S-1) 1951.

[8] L. Spitzer, "The Stellarator Concept," Phys. Fluids, 1, (1958) 253.

[9] C. Burnett, et al., "The divertor, a Device for Reducing the Impurity Level in a Stellarator," paper 359, Proc. 2nd UN Int. Conf. on the Peaceful Uses of Atomic Energy, Sept. 1958, Geneva, Switzerland, Vol. 32, Controlled Fusion Devices, 225.

[10] H. Hsuan, "Measurements of Plasma Flow Velocity into the Divertor of the FM-1 Spherator by Using Ion Acoustic Wave Propagation," Nuclear Fusion, 15 (1975) 191.

[11] DIVA Group, Nuclear Fusion, 18 (1978) 1619.

[12] A. V. Bortnikov, et al., 7th Intl. Conf. on Plasma Phys. and Cont. Nucl. Fusion Res., Innsbuck (1978) paper IAEA-CN-37/T-3-2.

[13] D. Meade, et al., 8th Intl. Conf. on Plasma Phys. and Cont. Nucl. Fusion Res., Brussels (1980) paper IAEA-CN-38/X-1.

[14] M. Keilhacker, et al., ibid.

[15] The ASDEX Team, "Divertor Experiments in ASDEX," IPP III/73, 10, 1981.

[16] D. Nagami, et al., 8th Intl. Conf. on Plasma Phys. and Cont. Nucl. Fusion Res., Brussels (1980).

[17] Various papers in Symposium on Energy Removal and Particle Control in Toroidal Fusion Devices, July 26-29, 1983, Princeton, NJ; Journal of Nuclear Materials 121 (1984).

[18] C. M. Colven, A. Gibson, P. E. Stott, in Proceedings of the 5th European Conf. in Contr. Fusion and Plasma Phys., Grenoble, 1972.

[19] K. B. Axon, et al., "The Bundle Divertor: A Review of Experimental Results," CLM-R235.

[20] K. B. Axon, et al., "Results from the DITE Experiment," 9th Intl. Conf. on Plasma Phys. and Contr. Fusion Res., Baltimore, 9, 1982, IAEA-CN-41/R-3.

[21] T. F. Yang, et al., "In Search of Optimized Bundle Divertors," PFC JA/81-4, October 1981.

[22] T. F. Yang, et al., "Optimization and Monte Carlo Modelling of Bundle Divertors," PFC JA/82-32, May 1983.

[23] L. M. Hively, et al., "Constrained Ripple Optimization of Tokamak Bundle Divertors," Nuclear Technology/Fusion, Vol. 2, July 1982, 372.

[24] P. E. Stott, et al., "The Bundle Divertor-Part II: Plasma Properties," Nuclear Fusion, Vol. 18, 4, (1978) 475.

[25] Intor Zero Phase, IAEA, Vienna (1980) 145.

[26] P. E. Stott, et al., "The Bundle Divertor-Part I: The Magnetic Configuration," Nuclear Fusion, Vol. 17, 3, (1977) 481.

[27] T. F. Yang, A. S. Wan, P. J. Gierszewski, "A Toroidal Hybrid Bundle Divertor for Alcator C," Bull. Am. Phys. Soc., 27 (18), 1982, paper 9W11.

[28] T. F. Yang, A. S. Wan, P. J. Gierszewski, "A Preliminary Bundle Divertor Design for Alcator DCT," PFC/RR-83-9, April 1983.

[29] J. L. Johnson, et al., "Numerical Determination os Axisymmetric Toroidal MHD Equilibrium," J. Comp. Phys, 32 (1979) 212.

[30] P. J. Gierszewski, A. S. Wan, T. F. Yang, "CCAN and TCAN-1 1/2-D Compressible-Flow and Time-Dependent Codes for Conductor Analysis," PFC/RR-83-1, January 1983.

[31] S. J. Sackett, "EFFI-A Code for Calculating the EM Field, Force, and Inductance in Coil Systems of Arbitrary Geometry," UCRL-52402.

[32] T. F. Yang, 5th Intl. Conf. on Magnet Technology, Frascati, 1975, paper MT-5, 203.

[33] T. F. Yang, et al., "Textor Bundle Divertor," PFC/RR-82-33, May 1982.

[34] ASDEX Upgrade Project Team, "ASDEX-UG, ASDEX Upgrade Project Proposal Phase II," IPP 1/217, May 1983.

[35] J. P. Freidberg, "Ideal MHD Theory of Magnetic Fusion Systems," Rev. of Modern Physics, Vol. 54, #3, July 1982, 801.

TABLE I

Basic Versator II Machine and Plasma Parameters

R_o = major radius = 40.5 cm

a = minor radius = 13.0 cm

B_o = TF on axis = 1.5 T

I_p = plasma current = 30.0 kA

n = line averaged density = 3 10^{13} cm^{-3}

T_{eo} = central electron temperature = 300-500 eV

T_{io} = central ion temperature = 120-170 eV

p = machine pulse period = 100 ms

FT = flat top time period = 30 ms

TABLE II

Preliminary Bundle Divertor Design Parameters for Versator II
(See Fig. 2 for variable definitions)

Coil	$_o$(cm)	(cm)	y (cm)	z (cm)	Cross Section(cm)		I(kA)
Divertor #1	56.0	5.0	6.0	16.0	2.5	2.5	74.0
Divertor #2	58.5	5.0	6.0	21.0	2.5	2.5	74.0
Divertor #3	61.0	5.0	6.0	26.0	2.5	2.5	74.0
Expander	69.0	4.0	7.5	26.0	3.0	3.0	111.5

TABLE III

Thermal Hydraulics Parameters for Versator Bundle Divertor Analysis Using TCAN

III.1 Coil Parameters

(See some variable definitions in Fig. 9 and other relevant parameters in Table II)

Coil	dx(cm)	dy(cm)	dins(cm)	r_{cool}(cm)	Total Length(cm)
Divertor #1	1.25	1.25	0.10	0.196	111.35
Divertor #2	1.25	1.25	0.10	0.196	133.57
Divertor #3	1.25	1.25	0.10	0.196	156.80
Expander	1.50	1.50	0.10	0.234	154.06

III.2 Coolant Parameters

Coolant = water

Total mass flow = 0.03 kg/s

Mass flux/coil = 2727.27 kg/m^2-s

Inlet pressure = 0.25 MPa

Inlet temperature = 290.0 K

III.3 Conductor Parameters and Other Relevant Parameters

Conductor = copper

RRR = 100

Magnetic field strength at coil = 4.0 Tesla

Pump hydraulic efficiency = 70%

TABLE IV

Results of the Thermal Hydraulics analysis for Versator Bundle Divertor Design

Coil	*1 $P_{electric}$(kW)	*2 $P_{refrigertor}$(kW)	ΔP(kA)	*3 T_{max}(K)	Total Req'd Energy (kJ)
Divertor #1	246.0	32.4	40	306.1	24.4
Divertor #2	295.2	38.8	40	306.1	32.8
Divertor #3	346.8	45.6	50	306.1	38.4
Expander	515.6	68.4	20	306.4	56.0
Total	1403.6	185.2	---	---	151.6

*1 Peak value, occurring at 110 ms into the pulse, right before the end of the flat top pulse in divertor current.

*2 Peak value, occurring early into the flat top pulse, typically around 20-50 ms after startup.

*3 Peak value at coolant exit, typically occurring a few msec after the end of the flat top pulse.

TABLE V

Poloidal Divertor and Equilibrium Coil Parameters

Coil	R(cm)	Z(cm)	I(kA)
Equilibrium #1	75.0	+41.0	-10.0
Equilibrium #2	75.0	-41.0	-10.0
Equilibrium #3	67.0	+45.0	-10.0
Equilibrium #4	67.0	-45.0	-10.0
Poloidal Divertor #1	30.0	+20.0	+25.0
Poloidal Divertor #2	30.0	-20.0	+25.0

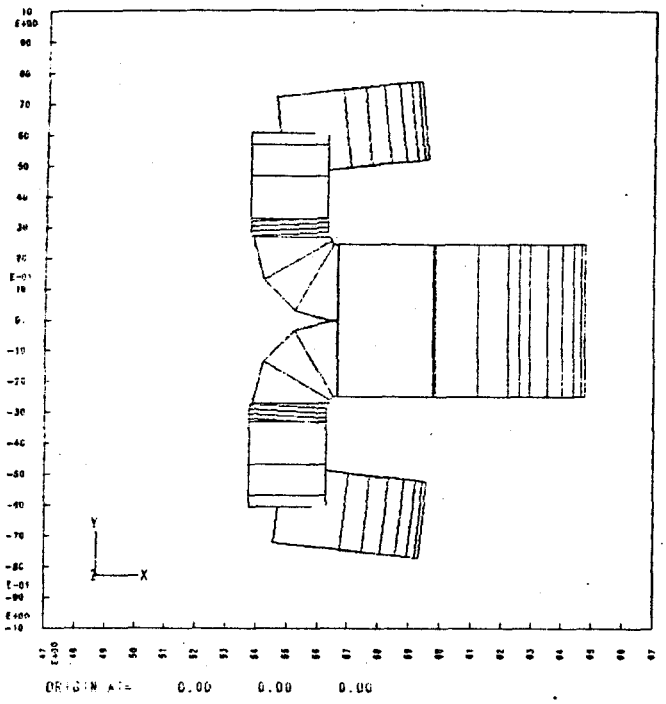

(a) Top View

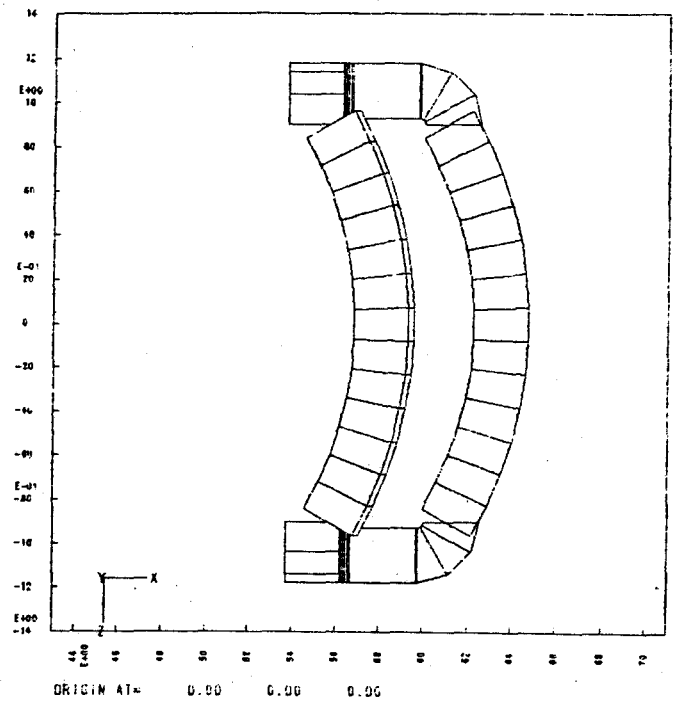

(b) Side View

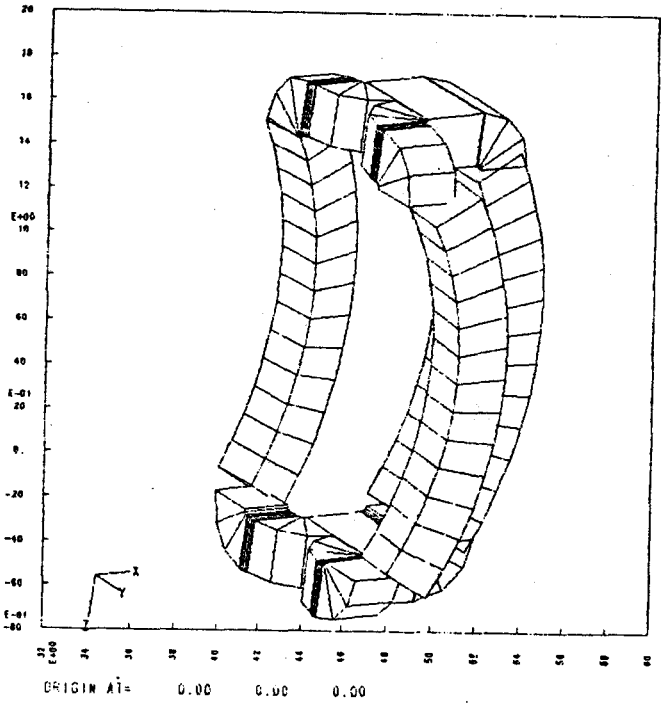

(c) 3-D View

Figure 1. Top, side, and 3-D views of a single arc-shape T-coil.

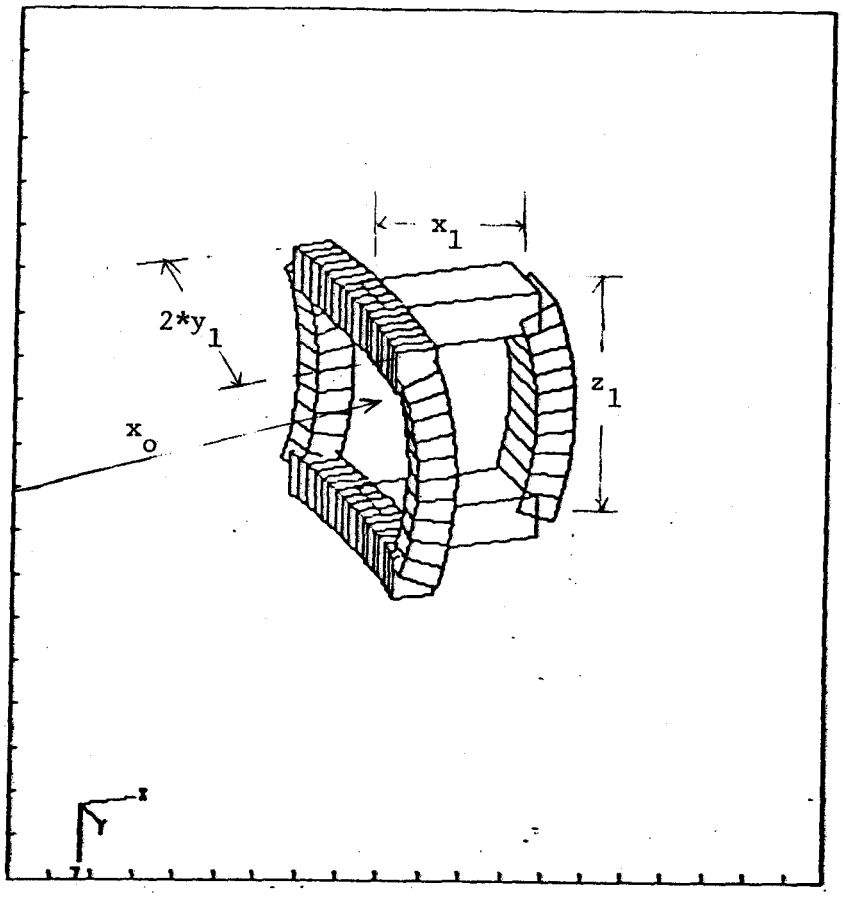

Figure 2. Single arc bundle divertor coil configuration with the design geometric variables. See Table 2 for the Versator bundle divertor parameters.

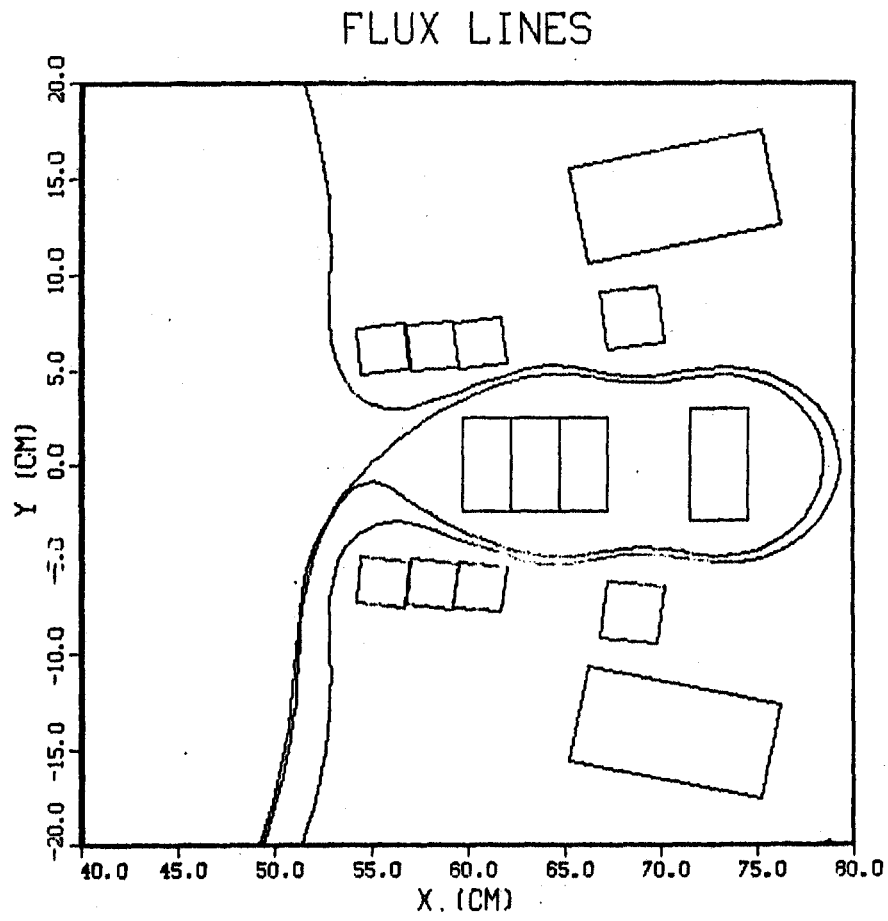

Figure 3. Magnetic flux configuration of the Versator bundle divertor. The separatrix is shown along with a field line launched near the edge of the scrape-off layer.

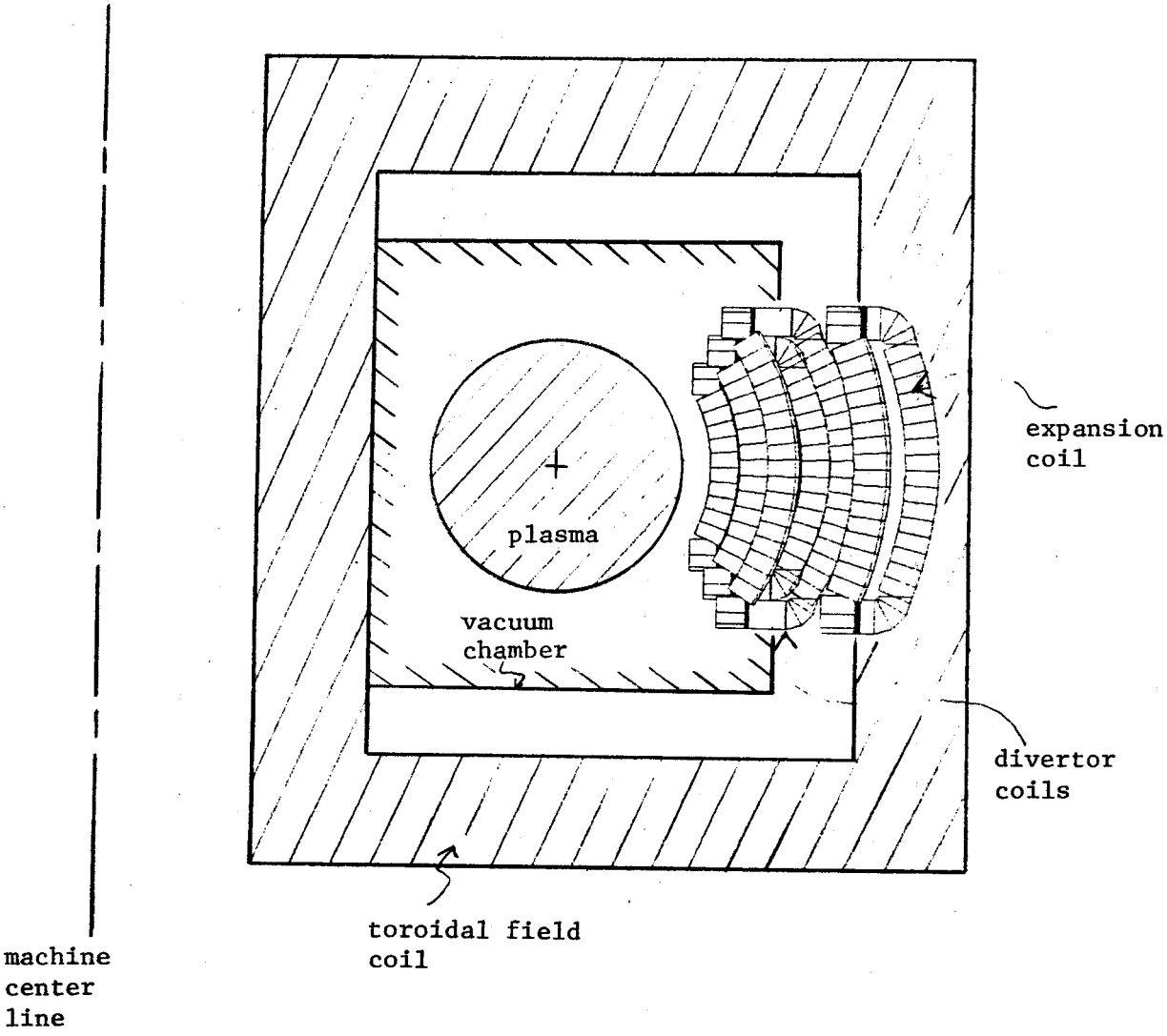

Figure 4. Relative positionings of the Versator toroidal field coil, the vacuum chamber, the plasma, and the designed bundle divertor with expansion coil.

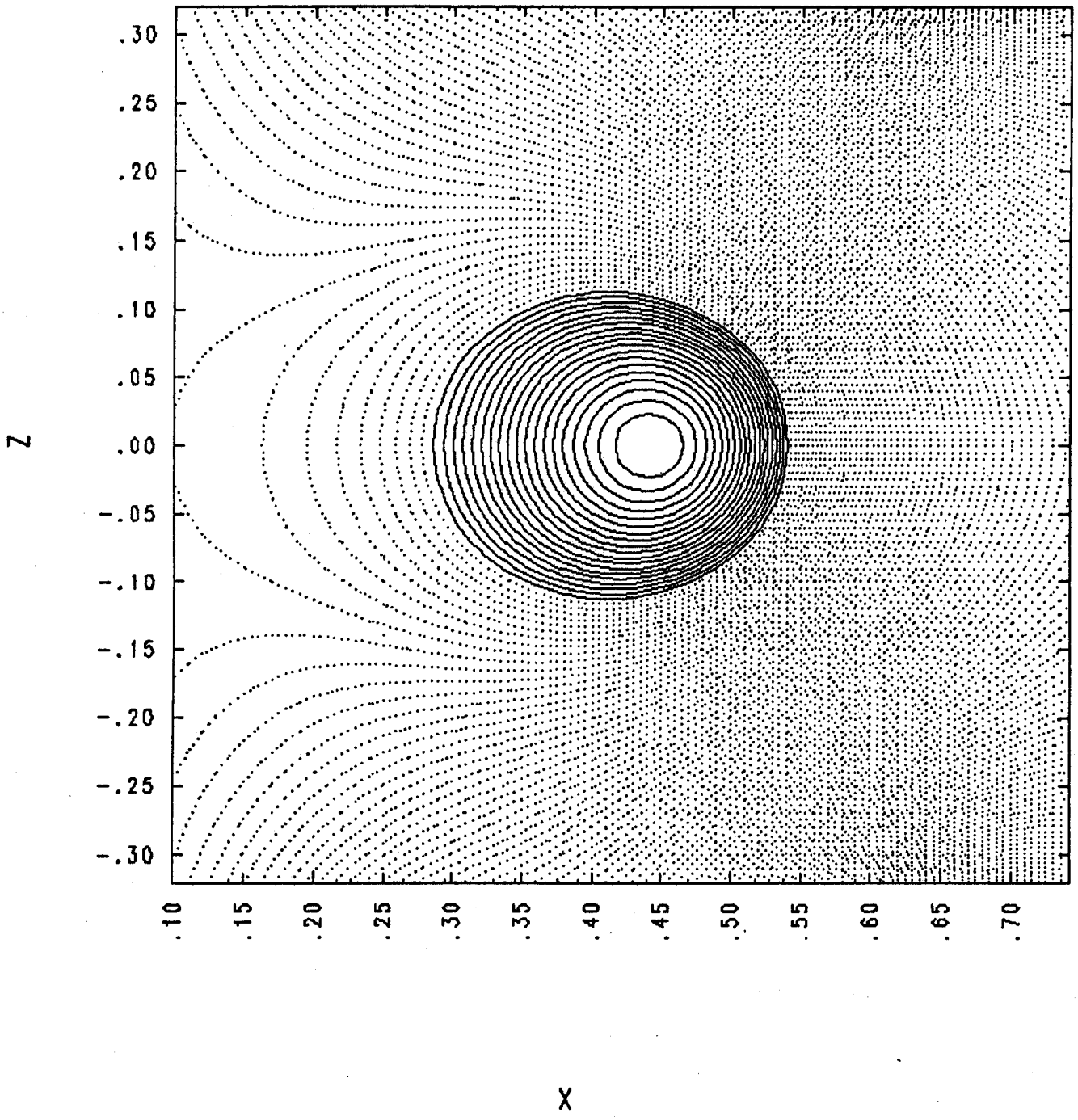

Figure 5. Contours of poloidal magnetic flux for the referenced equilibrium profile of Versator.

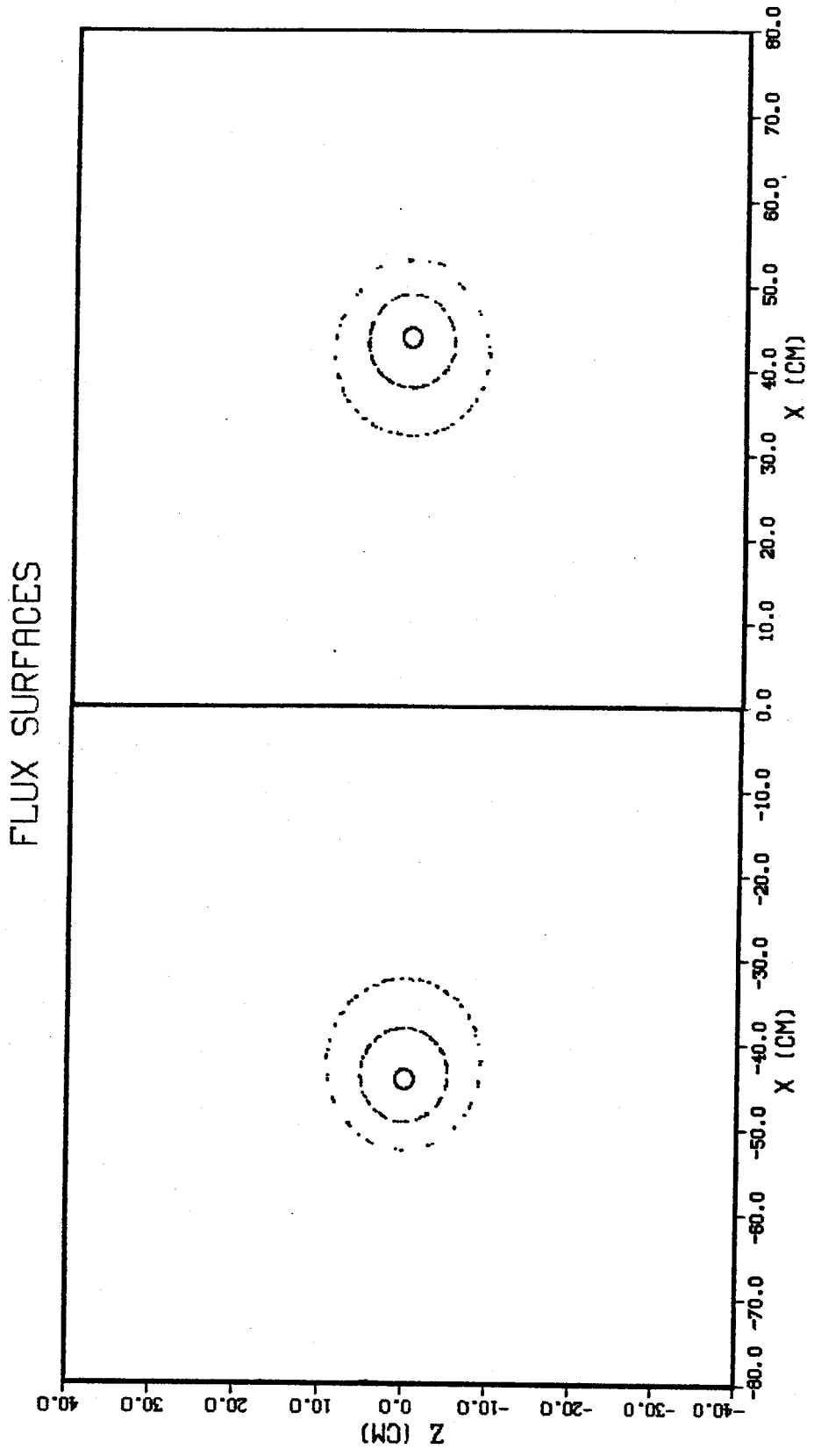

Figure 6. Puncture plot of the poloidal flux surfaces. The three flux lines are launched inside the separatrix and exhibited no ergodicity.

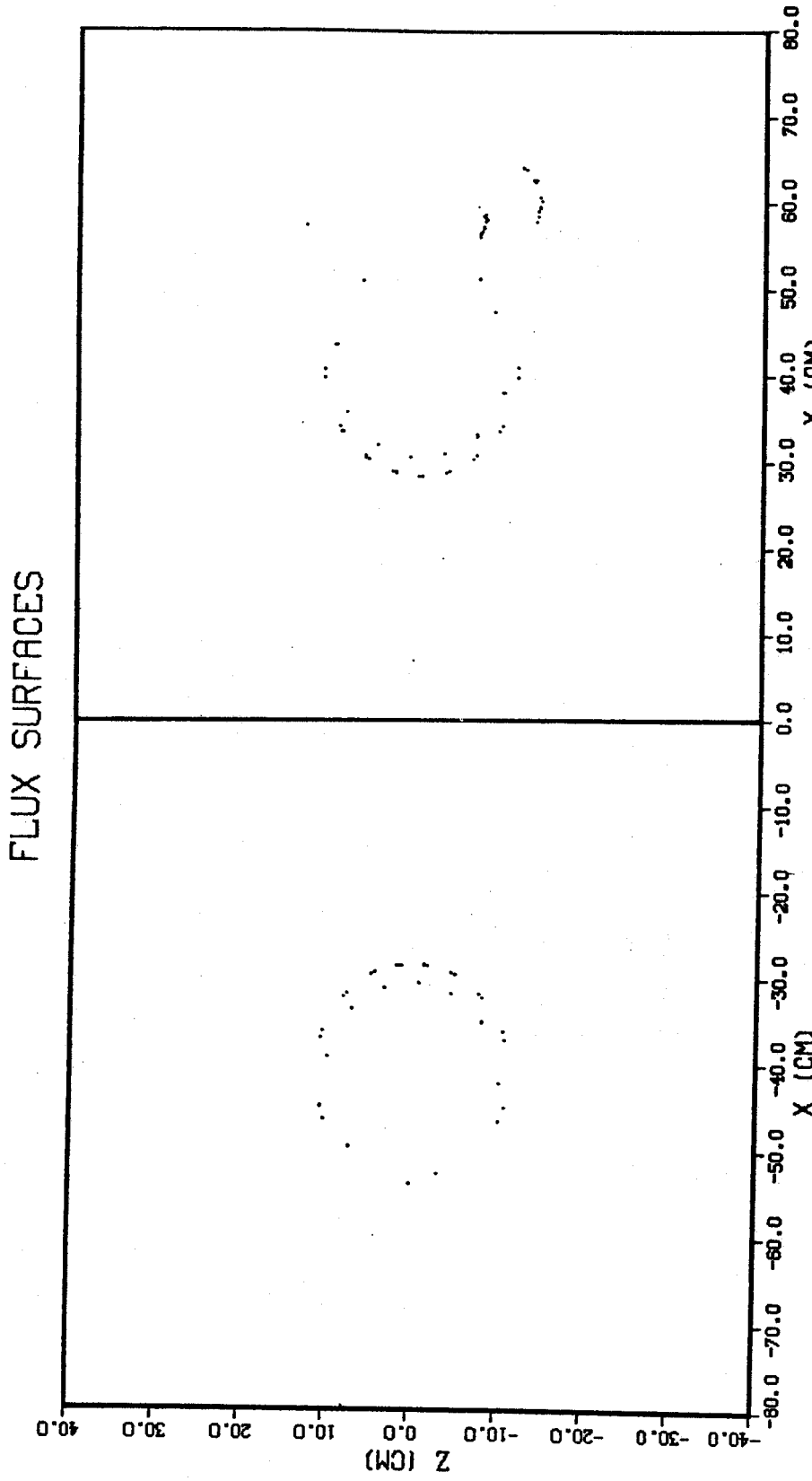

Figure 7. Puncture plot of the poloidal flux surface launched in the scrape-off layer. The field line is diverted into the divertor chamber and is trapped between the coils.

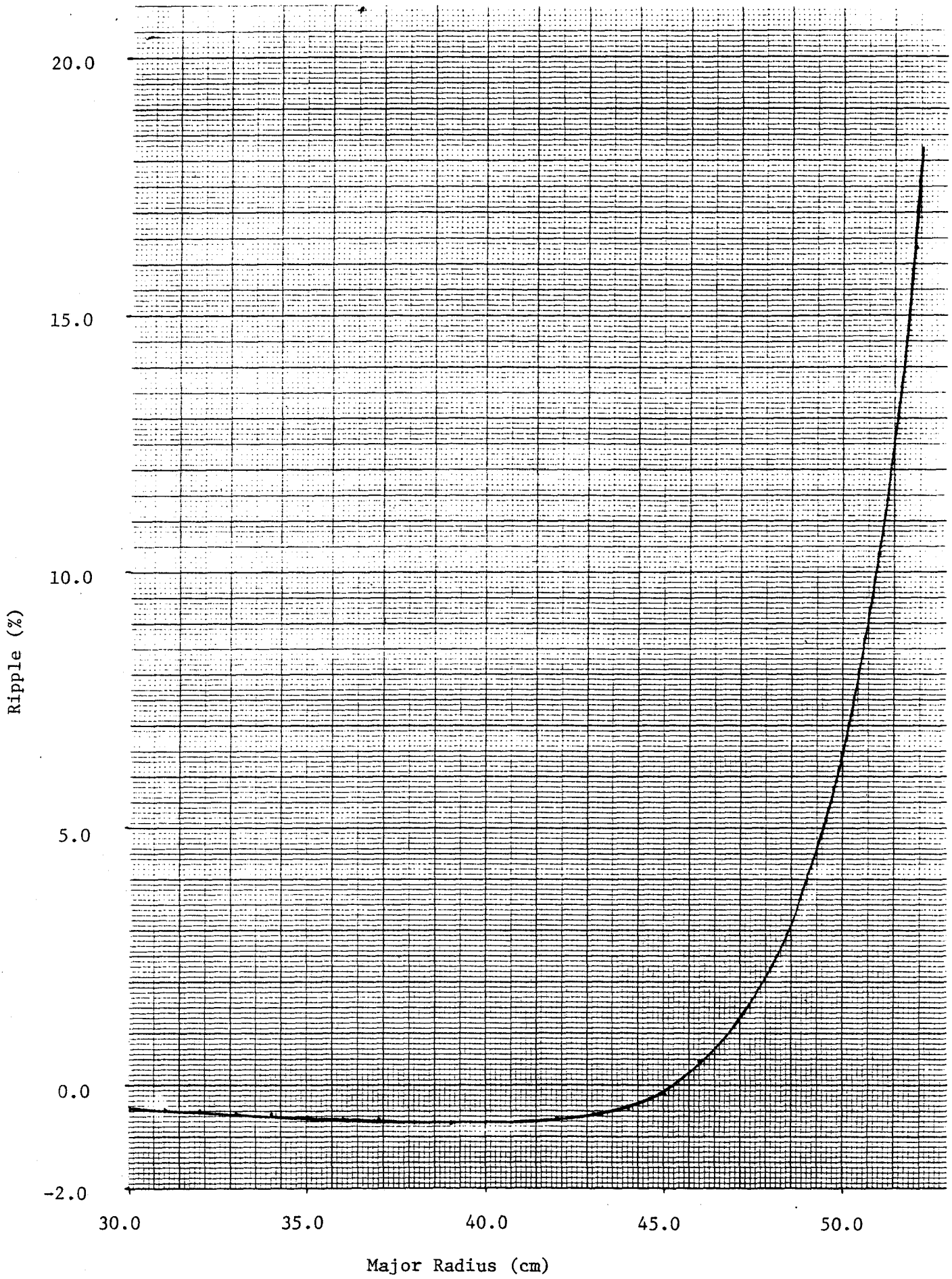

Figure 8. Ripple profile with Versator bundle divertor vs. major radius

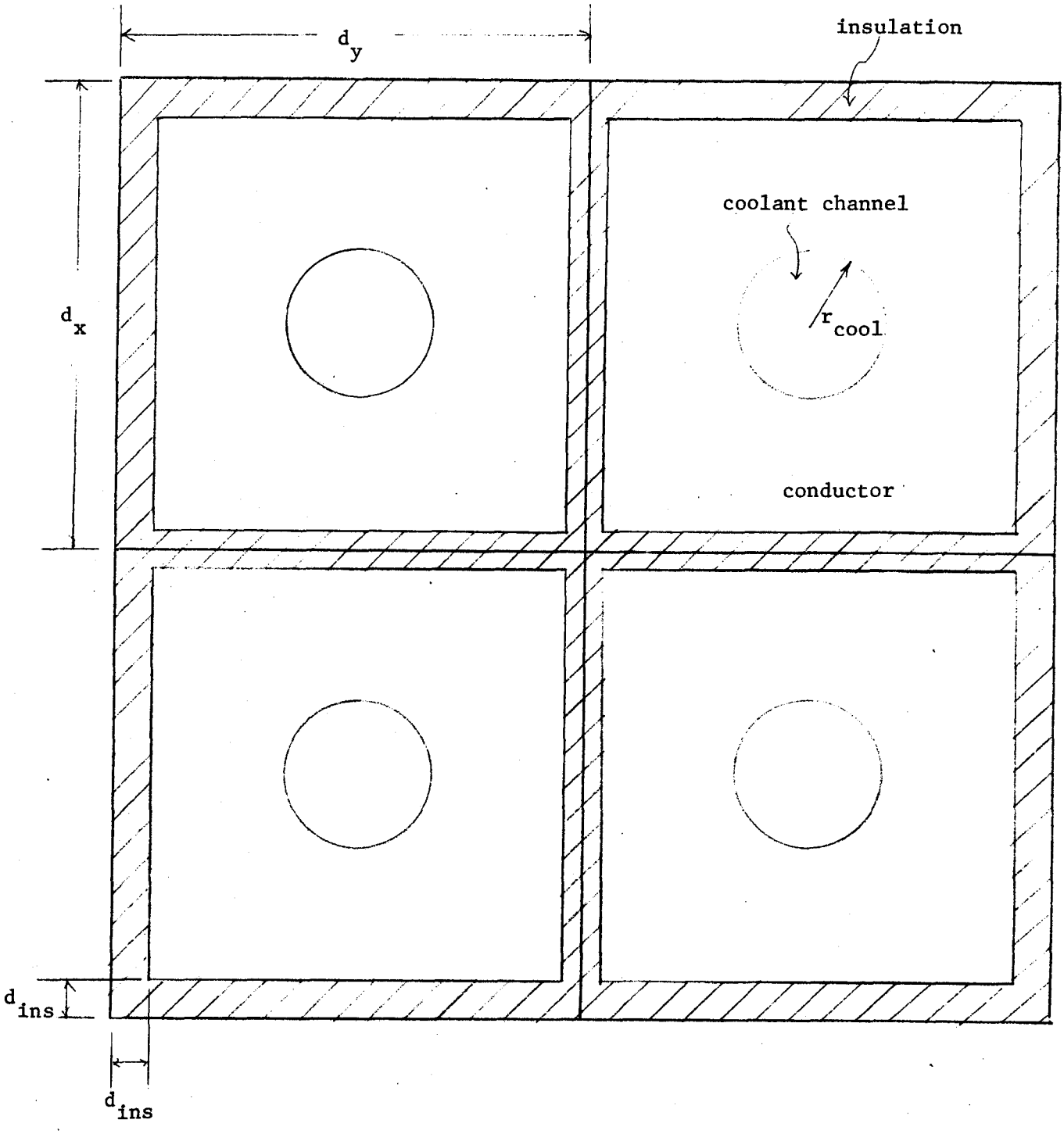

Figure 9. Coil cross-section for the thermal hydraulic analysis of the Versator bundle divertor design.
See design parameters in Table 3.

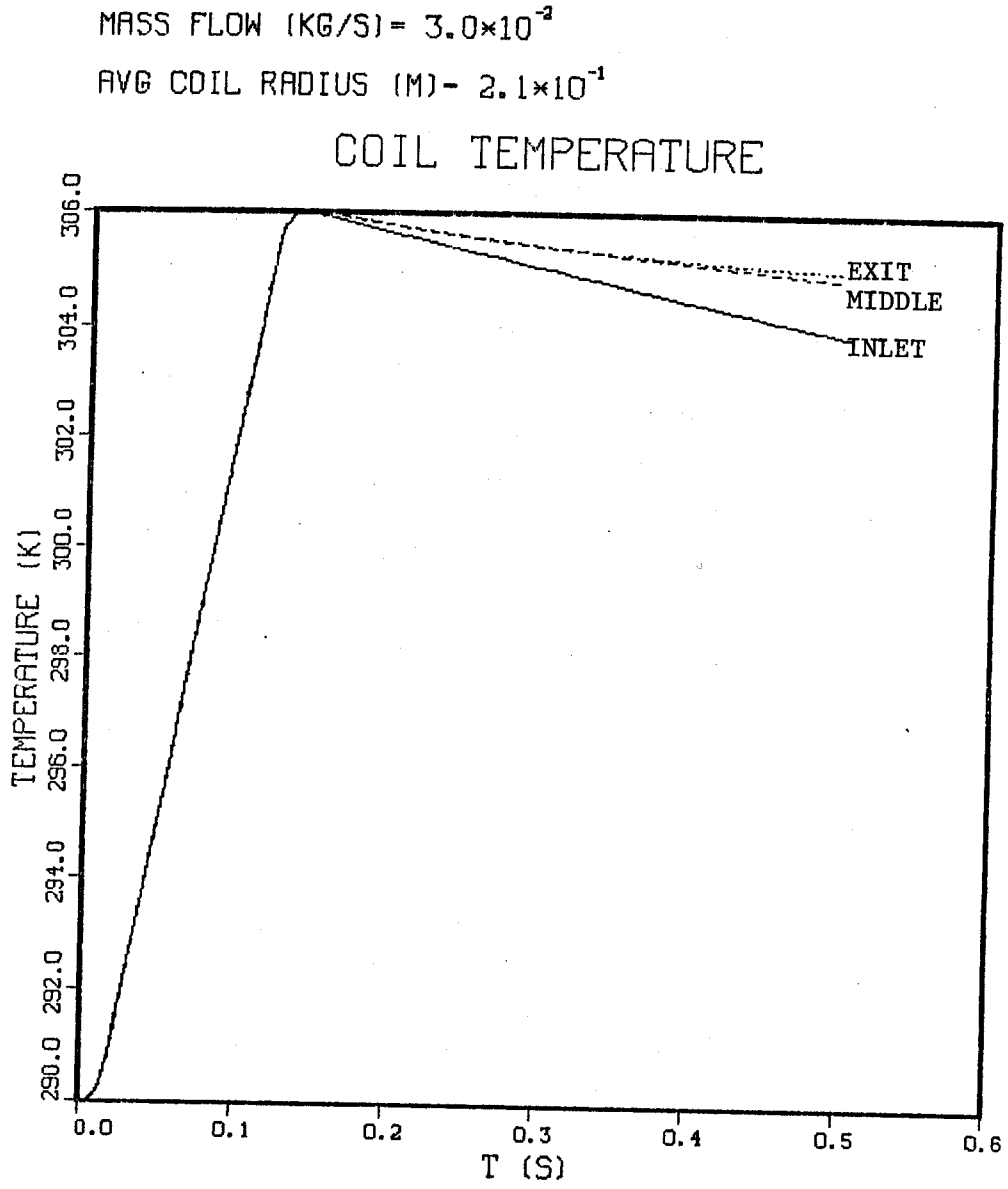

Figure 10. Time history of the temperature calculated (using TCAN) at the coolant inlet, coil mid-point (length-wise), and coolant exit for the second divertor coil.

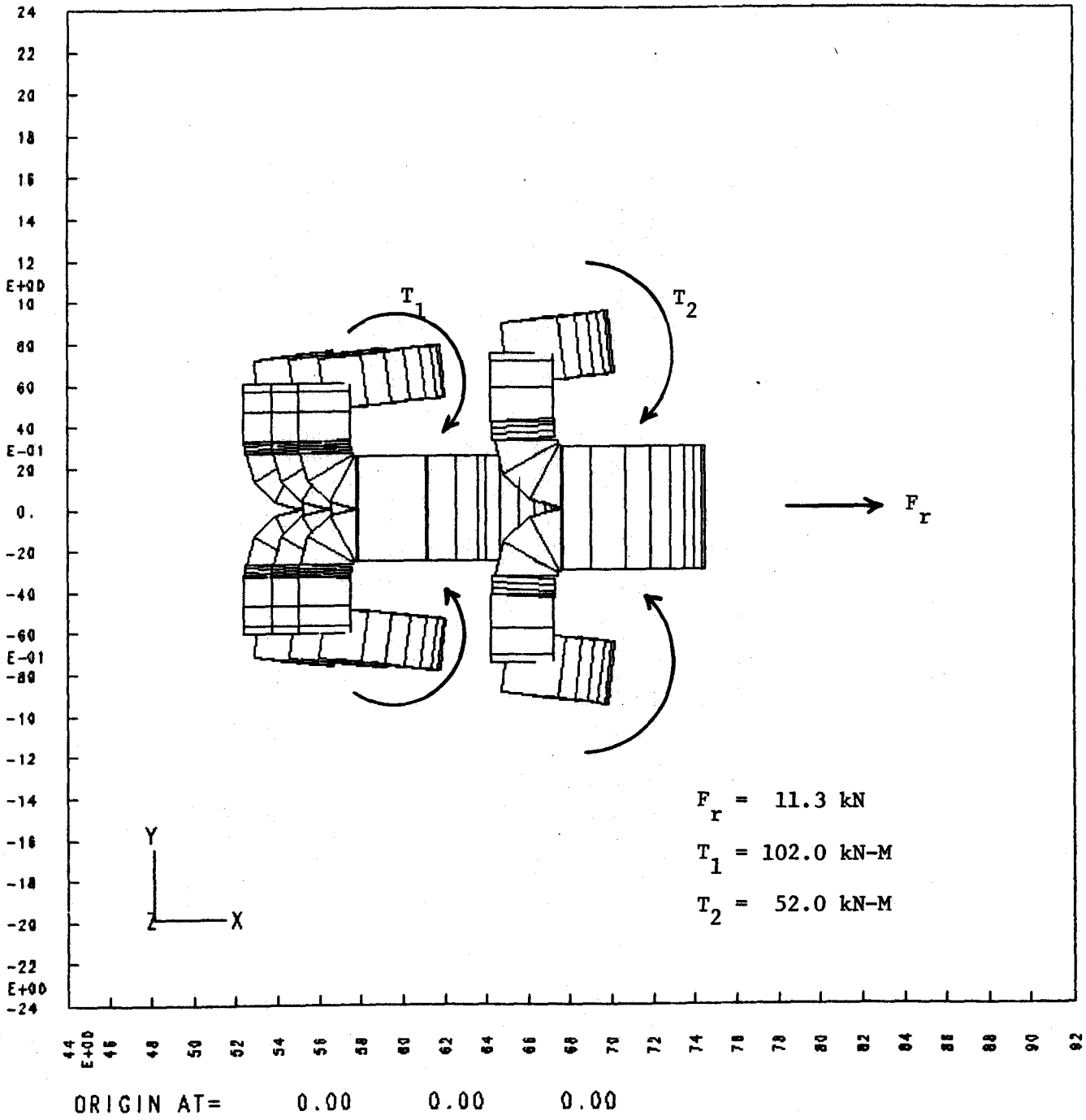

Figure 11. Total radial force (F_r), and torque on the main divertor coils (T_1) and on the expansion coils (T_2) for the Versator bundle divertor design.

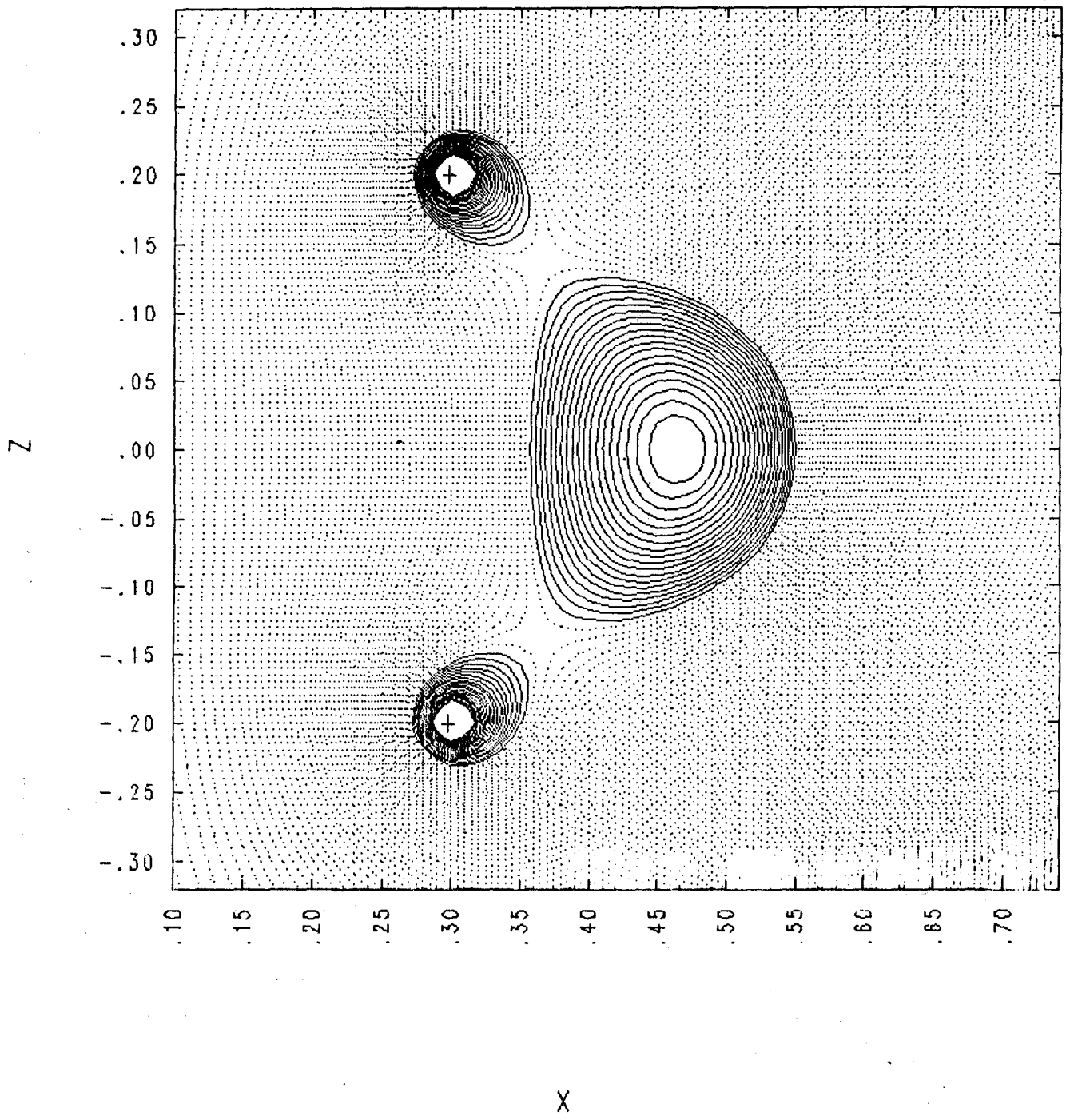

Figure 12. Contours of poloidal magnetic flux for the preliminary Versator poloidal divertor design. The poloidal divertor coils fit inside the vacuum chamber.